Forest Ecology and Management 486 (2021) 118945

Contents lists available at ScienceDirect

Forest Ecology and Management

journal homepage: www.elsevier.com/locate/foreco

Using terrestrial laser scanning for characterizing tree structural parameters and their changes under different management in a Mediterranean open woodland

Ekaterina Bogdanovich [a,*], Oscar Perez-Priego [a,b], Tarek S. El-Madany [a], Marcus Guderle [a], Javier Pacheco-Labrador [a], Shaun R. Levick [c], Gerardo Moreno [d], Arnaud Carrara [e], M. Pilar Martín [f], Mirco Migliavacca [a]

[a] Max Planck Institute for Biogeochemistry, Hans-Knöll-Str. 10, 07745 Jena, Germany
[b] Department of Biological Sciences, Macquarie University, 6 Wally's Walk, Sydney, NSW 2109, Australia
[c] CSIRO Land and Water, PMB 44, Winnellie, Darwin, NT 0822, Australia
[d] Forest Research Group – INDEHESA University of Extremadura, 10600 Plasencia, Spain
[e] Fundación Centro de Estudios Ambientales del Mediterráneo (CEAM), Charles Darwin 14, Parc Tecnològic, 46980 Paterna, Spain
[f] Environmental Remote Sensing and Spectroscopy Laboratory (SpecLab), Spanish National Research Council (CSIC), Albasanz 26-28, 28037 Madrid, Spain

ARTICLE INFO

Keywords:
TLS
Iberian dehesas
Fertilization
Pruning
Tree crown
Multitemporal

ABSTRACT

Analyzing tree structural features and capturing their temporal dynamic is challenging but crucial for determining key state variables related to plant function, management practices, and aboveground vegetation stocks. Terrestrial laser scanning (TLS) provides a mean for representing those key variables in three-dimensional space and through time.

Here we further developed and tested two point cloud slice-based methods for estimating diameter at breast height (DBH) based on how the delineation of the slices of the tree stem point cloud was performed: the first method was based on the circumference of a slice (CM), and the second method was based on the average diameter of a slice (PM). Further, we focused on the characterization of three tree structural properties from TLS: maximum tree height (h_{max}), crown projected area (CA), and DBH, and then on the evaluation of their biometric relationships. Finally, we tested the potential of multitemporal TLS for evaluating the impact of tree management on tree structural properties and growth in a Mediterranean open woodland. In particular, we evaluated the effect of tree pruning and fertilization on h_{max} and CA.

The study was conducted in three plots exposed to different fertilization treatments in a Mediterranean open woodland with ≃20% of fractional cover of evergreen holm oak (*Quercus ilex L.*): a control treatment without fertilization, a Nitrogen addition treatment, and a Nitrogen plus Phosphorus addition treatment. Pruning effects on tree growth were assessed in two plots within the control: an unpruned area and an area pruned in 2005.

Estimation of the DBH showed a good agreement with field measurements ($R^2 = 0.93$ for PM and $R^2 = 0.94$ for CM). Despite *Quercus ilex L.* being characterized as a slow-growing species, a temporal difference of three years among TLS was sufficient to quantify the influence of different management strategies on tree structural properties and growth rates. Our results showed: (i) CA increased relatively more than $h_{max,}$ independent of the respective management strategy, suggesting a preferential lateral growth in holm oak tree canopies in this open woodland, (ii) pruned trees showed larger changes in CA than control trees (Wilcoxon test $p < 0.01$), whereas fertilized trees grew more in height compared with control trees (Wilcoxon test $p < 0.01$), and (iii) biometric relationships among plant properties were affected by nutrient fertilization and pruning. These results show that

Abbreviations: CA, crown projected area; h_{max}, maximum tree height; TD, tree density; DBH_{TLS}, diameter at breast height, derived from TLS; DBH_f, diameter at breast height, measured in field; DBH_d, diameter at breast height, measured with a dendrometer; CM, circumference method; PM, perpendiculars method; CT, Control treatment, no fertilization; CT_nP, Control treatment, no fertilization, no pruning; CT_P, Control treatment, pruned trees; NT, Nitrogen treatment; NPT, Nitrogen and Phosphorus treatment.

* Corresponding author at: Max Planck Institute for Biogeochemistry, Hans-Knoell-Str. 10, 07745 Jena, Germany.
E-mail address: ebogdan@bgc-jena.mpg.de (E. Bogdanovich).

https://doi.org/10.1016/j.foreco.2021.118945
Received 21 August 2020; Received in revised form 22 December 2020; Accepted 11 January 2021
Available online 11 February 2021

multitemporal TLS shows promise for monitoring even small changes in crown dimensions, and it is a valuable tool for conducting vegetation dynamics studies and quantifying management effects.

1. Introduction

Accurately quantifying the dynamics and structure of vegetation is necessary to understand the ecological processes underlying ecosystem functioning, as well as the effect of human activities and management. State variables of vegetation, such as plant height, plant volume, and the diameter at breast height (DBH), as well as their spatial distribution and cover, are fundamental in ecosystem research and modeling of plant functional types, diversity, carbon accounting, and ecophysiology (Houghton et al., 2001; Chave et al., 2005; Hayat et al., 2017; Pommerening and Grabarnik, 2019). Biometric relationships between plant height and diameter are used for estimating terrestrial biomass, which plays an essential role in carbon cycling (Houghton et al., 2009). The dynamics of vegetation structure, such as stem and canopy growth, are typically used as an indicator of vegetation function, which is mediated by environmental forcing and human activities, such as management. Some of the standard management practices aimed at increasing tree growth or fruit yield include fertilization and structural pruning. A robust characterization of structural canopy properties and their dynamics is necessary to assess whether management strategies are successful.

Light detection and ranging (LiDAR) active sensors have been successfully used to estimate vegetation structural parameters in a variety of ecosystem types. The substantial advantage of these sensors over passive sensors is their ability to reproduce the 3D structure of a given target independently on an external illumination source (Lefsky et al., 2002; Hill et al., 2011). LiDAR instruments are operated from a variety of platforms. Spaceborne LiDAR is used primarily for land cover classification and the estimation of ice, sea, and terrain elevation at the global scale. Airborne laser scanning (ALS), ground-based LiDAR, which is also known as terrestrial laser scanning (TLS), mobile laser scanners (MLS), Hand-Held Mobile Laser Scanning (HMLS), unmanned aerial vehicles (UAV) laser systems provide information about terrain and vegetation structure at the scale of single tree elements to the whole ecosystem (van Leeuwen and Nieuwenhuis, 2010). LiDAR instruments have been used to estimate tree structural parameters, such as height (Hopkinson et al., 2004; Popescu et al., 2004; Popescu and Zhao, 2008; Lin et al., 2010; Moskal and Zheng, 2011; Olofsson et al., 2014; Srinivasan et al., 2015; Liu et al., 2018), crown diameter (Popescu et al., 2004; Popescu and Zhao, 2008; Yao et al., 2012; Srinivasan et al., 2015; Herrero-Huerta et al., 2018), and tree volume (Bienert et al., 2014; Herrero-Huerta et al., 2018; Putman and Popescu, 2018). DBH is one of the essential parameters for estimating tree basal area and biomass via allometric scaling. Whilst ALS can provide DBH estimations based on allometric equations in some system (Popescu et al., 2004; Yao et al., 2012), TLS provides a more direct measurement through circle and cylinder fitting (Hopkinson et al., 2004; Bienert et al., 2007; Moskal and Zheng, 2011; Srinivasan et al., 2015; Ravaglia et al., 2019).

Seasonally dry tree-grass ecosystems, including savannas, are globally widespread, and their functioning plays an important role in determining the interannual variability of global carbon dioxide (CO_2) fluxes (Poulter et al., 2014; Ahlström et al., 2015). Therefore, it is

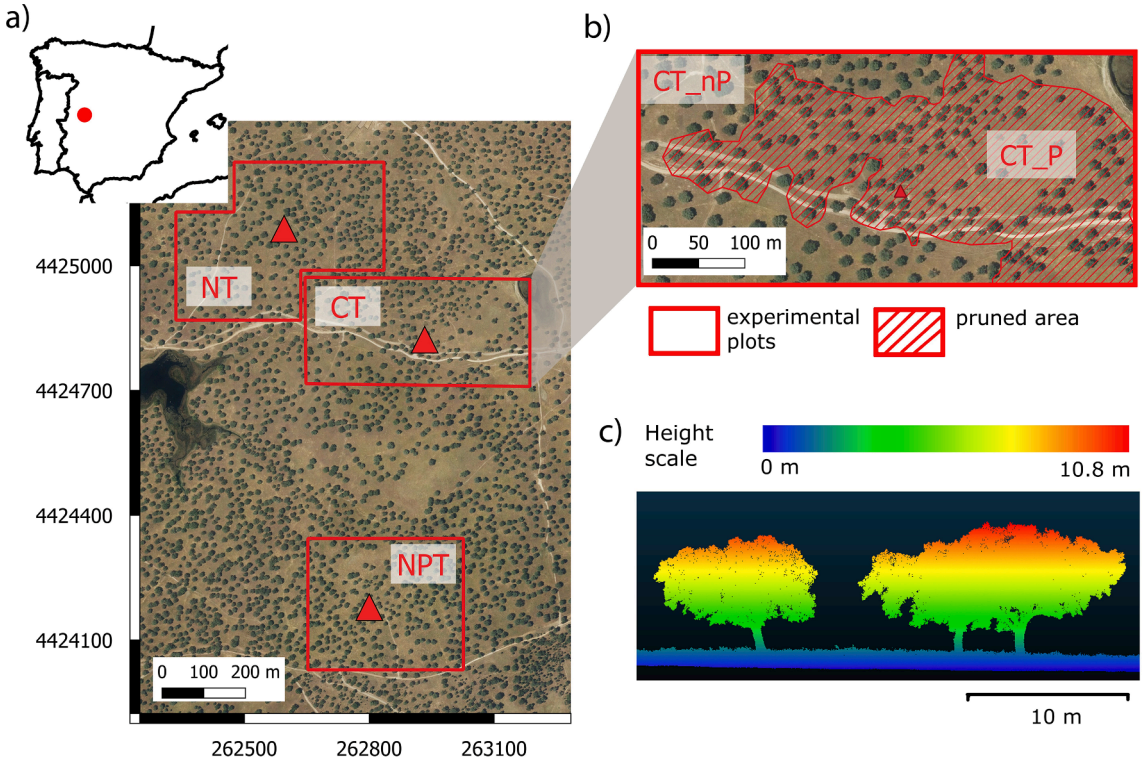

Fig. 1. The study site Majadas de Tiétar. (a) location of the study site in Spain (red point) and an orthophotograph in UTM projection with locations of three fertilization experiments (red boxes): CT - control treatment (no fertilization), NT – nitrogen added treatment, NPT – nitrogen and phosphorus added treatment; red triangles – eddy covariance flux towers location; (b) CT plot was separated in two regions: unpruned area (CT_nP or control trees) and pruned area (CT_P, pruned trees); (c) TLS point cloud cross-section. The true-color RGB orthophotograph image used in a and b was provided by the Spanish National Orthophotography Program (PNOA in Spanish) database. The spatial resolution is 25 cm, the acquisition year is 2016. (For interpretation of the references to color in this figure legend, the reader is referred to the web version of this article).

important to monitor the structural properties of savanna ecosystems through time and assess their response to management practices. Semi-arid savannas are characterized by sparsely distributed trees, with 10–40 trees/ha typically, which makes them suitable for efficient characterization with LiDAR. Both ALS and TLS accurately characterize the structural features of savanna vegetation. For example, Chen et al. (2006) applied an ALS-derived canopy height model (CHM) to delineate trees in open oak-savanna in California. The combination of ALS and hyperspectral data was used for classifying and mapping tree species in African savannas (Cho et al., 2012; Colgan et al., 2012; Naidoo et al., 2012). TLS has been used to estimate biomass (Zimbres et al., 2020) and tree structural properties (Muir et al., 2018) and for the characterization of the distribution of leaves inside the tree canopy (Béland et al., 2011; García et al., 2015). Both ALS and TLS are valuable for assessing the impact of management actions, such as controlled burning, on vegetation structure in savannas (Levick et al., 2015; Singh et al., 2018; Levick et al., 2019).

Mediterranean open woodlands, which are also called *"Iberian dehesa"* are tree-grass ecosystems with high socioeconomic and environmental value primarily located in the Central-West Iberian Peninsula. They are formed by thinning dense oak forests, and they are maintained by grazing the grass understory and through the periodical pruning of sparse trees. Holm oak (*Quercus ilex L)* is one of the key tree species occupying Mediterranean landscapes (Huntsinger et al., 2013). Periodical pruning is conducted to shape the tree canopy to maximize light interception and acorn production, which is a preferred forage resource of livestock (Joffre et al., 1999). Monitoring tree growth is a challenging task, especially for slow-growing tree species, such as the holm oak. Consequently, different measurable proxies for tree growth have been used in the past. For instance, most studies determine holm oak growth using multitemporal dendrometer measurements of tree stem diameter (Mayor and Rodà, 1994; Martin et al., 2015) or manual measurements of shoot length (Pulido et al., 2013). However, these metrics do not provide an overview of whole-tree growth. Multitemporal LiDAR surveys provide an opportunity to detect changes in vegetation structure at a high spatial resolution in three dimensions. For example, ALS has been used to determine forest decline, tree loss, and tree growth through height and biomass changes in mixed and conifer forests (Yu et al., 2006; Hopkinson et al., 2008; Duncanson and Dubayah, 2018). Multitemporal ALS has also been used for monitoring structural changes in vegetation in savannas (Levick and Asner, 2013). However, the accuracy of changes detection is limited by measurements uncertainty, and for quantifying fine-scale changes the use of multitemporal TLS offers advantages in resolution and precision over ALS.

This study aimed to evaluate the potential of multitemporal TLS to estimate tree structural parameters of holm oak trees in a Mediterranean open woodland and to measure the impact of management actions on tree growth. We decided to focus on three key state variables, maximum tree height (h_{max}), crown projected area (CA), and DBH. These variables are widely used for characterizing of stand structure (Valladares and Guzmán, 2006), allometric equations (Henry et al., 2011; Forrester et al., 2017), and modeling (Chave et al., 2005; Hayat et al., 2017). We have three specific objectives: (i) to develop tree stem slice-based methods further to estimate DBH for holm oak, (ii) to characterize the variability of TLS-derived biometric relationships between maximum tree height (h_{max}), crown projected area (CA), and DBH, to define the structural composition of a Mediterranean open woodland and (iii) to investigate the impact of pruning and fertilization treatments on tree growth by focusing on variations in h_{max} and CA.

2. Material and methods

2.1. Study site

The study site is located in western Spain (39°56′024.68″N, 5°45′50.27″W; Majadas de Tiétar, Cáceres, Extremadura; Fig. 1a). The ecosystem type is a Mediterranean open woodland with a Mediterranean climate, characterized by a hot, dry summer, annual precipitation of ~650 mm, which falls mostly in spring and autumn, and mean annual temperature of ~16 °C. The understory is dominated by a grass layer of *Vulpia bromoides (L.), Vulpia geniculate (L.), Trifolium subterraneum (L.),* and *Ornithopus compressus (L.)*. The woody vegetation is dominated by the evergreen holm oak, *Quercus ilex L.*, with a low tree density of ~20 trees per ha, with an average height of 8 m and an average DBH of 0.4 m. The holm oak is a slow-growing species, and it has a dense canopy and small coriaceous leaves (Terradas, 1999). Vegetative growth occurs primarily during spring and occasionally late in autumn.

The site is managed by low-intensity grazing of < 0.3 cows per ha (Perez-Priego et al., 2017; El-Madany et al., 2018), as is typical for *Iberian dehesas*. The trees at the study site were pruned every 20–25 years to maximize acorn production as forage for livestock.

2.2. Fertilization experiment and management

We made use of a large scale (~24 ha) nitrogen and phosphorous fertilization experiment conducted in 2015 (Nair et al., 2019; Luo et al., 2020) on three different plots (Fig. 1a): the control treatment (CT), the Nitrogen treatment (NT) and the Nitrogen plus Phosphorus treatment (NPT). We covered with TLS a portion of each treatment: 13.3 ha for CT, 14.9 ha for NT, and 11.8 ha for NPT. All the plots were equipped with eddy covariance flux towers (El-Madany et al., 2018).

Some trees on the CT plot were pruned in 2005, and we analyzed the changes in tree structural characteristics in the 6.4 ha unpruned (CT_nP or control trees, n = 30) and 6.9 ha pruned areas (CT_P, pruned trees, n = 42) (Fig. 1b).

2.3. Data

2.3.1. Terrestrial laser scanning data

We conducted two TLS surveys in the three plots using a Riegl VZ-2000 laser measurement system (Riegl Laser Management Systems GmbH): the first was between the 19th and 21st of August 2015, and the second was between the 21st and 26th of October 2018. The Riegl VZ-2000 is a full-wave TLS system that operates in the near-infrared region of spectrum (1500 nm wavelength), with a maximum of 360° horizontal and 100° vertical field-of-view. Our scans were conducted at 0.02 mrad and 550 kHz with a maximum ranging ambiguity of 750 m. In 2015, the TLS sensor was installed on a tripod at a height of ~1.80 m. Data acquisition covered an area of 67 ha and included 113 randomly selected scanning locations (Fig. A1 in appendix). In 2018, we modified the acquisition scheme to reduce occlusion that was observed in the 2015 data, which could lead to the underestimation of tree structural parameters. The acquisition scheme in 2018 was implemented in a regular predefined grid with a ~ 80 m distance between scan locations, which resulted in 174 scanning locations covering 76.16 ha (Fig. A1 in appendix). The scanner was mounted on a vehicle at a height of ~2.20 m. The acquisition patterns in 2015 and 2018 resulted in point densities of 1186 and 3372 points per m^2 respectively for all returns. For both years, the last sprout had occurred in the previous spring (April-May) at the time of field scanning, and the stem and branches were not growing.

2.3.2. Orthophotographs

Field measurements of CA in *dehesa* are error-prone because of the irregular shape of the tree crown and its large size (Husch et al., 2002). Thus, we used an orthophotograph for inter-comparison with the CA derived from the 2015 TLS. The true-color RGB orthophotograph was provided by the Spanish National Orthophotography Program (PNOA in Spanish) database. The orthophotograph, with a spatial resolution of 25 cm, was acquired in 2016 during the dry season. We randomly selected 36 trees among those that were unoccluded in the TLS point clouds in 2015 (Fig. A2 in appendix), and we manually delineated tree crowns on the orthophotographs based on the spectral difference with the

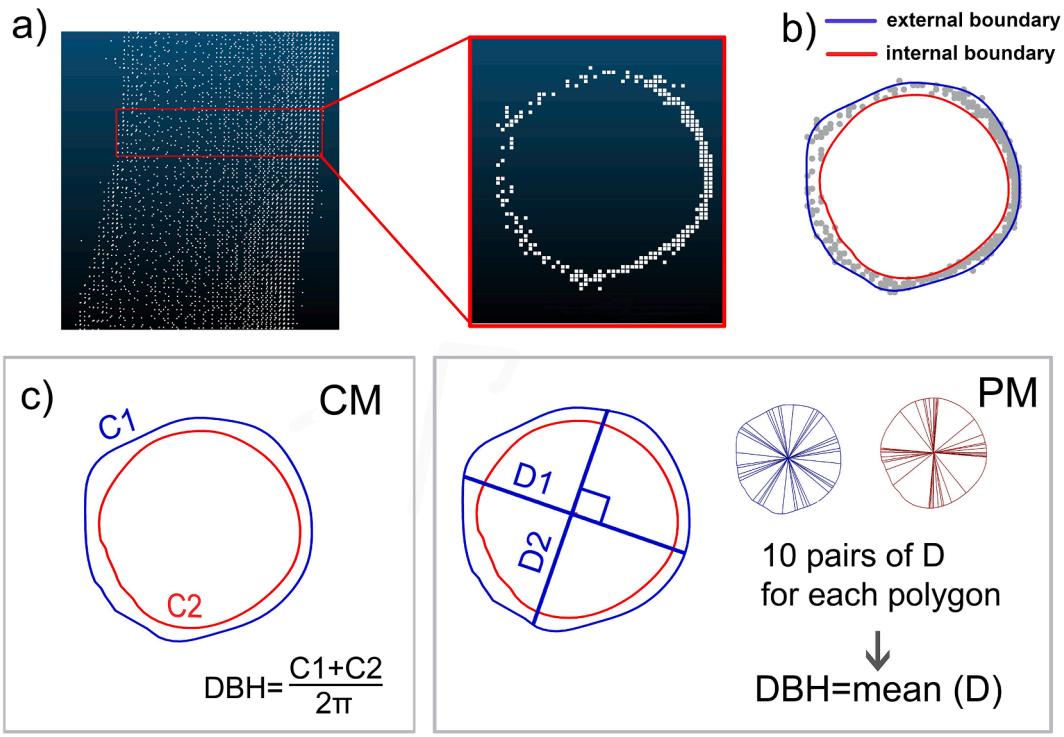

Fig. 2. DBH estimation from TLS scans. (a) Left: TLS point cloud of a tree stem. The red polygon indicates the approximated location of DBH measurements (1.25–1.35 m); right: Point cloud of sliced stem (up-down view) (b) result of delineation: external boundary is in blue color and internal boundary is in red color (c) calculation methods: CM – circumference method, PM - perpendiculars method. C is circumference, D is diameter. (For interpretation of the references to color in this figure legend, the reader is referred to the web version of this article).

background of dry grass and shadows. CA was then calculated using QGIS software (QGIS Development Team, 2019).

2.3.3. Field measurements of the diameter at breast height and dendrometer data

We used field observations of DBH (DBH_f) acquired in 2015 to ground-validate the DBH derived from TLS (DBH_{TLS}) and to establish the biometric relationships between tree parameters. We sampled >900 trees in the study site using a tree caliper at the height of 1.30 m.

Dendrometer bands were installed around the stems of 10 selected holm oak trees (Fig. A2 in appendix) at a height of 1.30 m above the ground at the permanent tree girth band D1 (UMS GmbH) to follow the temporal dynamic of DBH. Changes in the circumference of the trees were manually recorded up to five times per year. Six additional trees were equipped with stand-alone logging dendrometer bands DBL60 ICT (ICT international) to obtain a higher temporal resolution (Fig. A2 in appendix). Among trees equipped with dendrometers 4 trees were fertilized, 10 trees were pruned, and 2 trees were control ones. We extracted the circumference values closest to the TLS surveys: 19/08/2015 and 24/10/2018 for automatic dendrometers, 22/05/2015 and 24/10/2018 for the manual ones. Then, the DBH at the time of the scan was calculated by dividing the actual circumference value by π (DBH_d). We recalibrated the manual readings to account for temporal differences between the manually acquired data and TLS data. We observed a growth of 0.02 cm with the automatic dendrometers for this temporal frame. The calculation of the relative change in DBH_d between 2015 and 2018 is explained in Section 2.7.

2.4. Terrestrial laser scanning data pre-processing

The 2015 and 2018 TLS datasets were processed in the same way, using the multi-station adjustment tool in RiSCAN Pro (Riegl Laser Management Systems GmbH) for co-registration. Further post-processing steps were implemented using LAStools (rapidlasso GmbH, 2007–2019). First, we clipped the TLS point clouds according to the reference plots (Fig. 1a) to analyze common areas for the two datasets. After classifying the TLS returns to ground and non-ground points, the z-coordinate of non-ground points was normalized to the height above ground level. For the height calculation, we generated a CHM using the normalized non-ground returns with a rasterizing of the triangulated irregular network (TIN) (Axelsson, 2000) to a 0.05 m grid spatial resolution. An interpolated CHM, with the same resolution, was used to calculate the CA following the approach of Isenburg (2014), which is based on Khosravipour et al. (2014). The advantage of interpolated CHM is the absence of "pits," which are empty pixels inside tree canopies on the standard CHM, which obstruct tree crown delineation. The interpolated CHM is a combination of several standard CHMs, which are generated by interpolating the highest returns below a certain height using a TIN (Axelsson, 2000). Thus, each of the standard CHMs represents only part of the canopy, and their further emergence allows the generation of smoothed rasters, which are known as interpolated CHMs. We generated nine standard CHMs using the LAStools "las2dem" tool, one "ground" CHM to fill the potential holes on the ground level, with an interpolation of the highest returns below 0.1 m, one "initial" CHM, with an interpolation of all the highest returns to fill the potential holes at the vegetation level, and seven CHMs with interpolation steps 1, 2, 5, 10, 12, 15, and 20 m. Then, we used the LAStools "lasgrid" tool to merge all standard CHMs into one interpolated CHM.

2.5. Selection of trees

For the characterization of tree structural parameters and temporal analysis we selected only those trees for which we had the complete coverage of the point cloud for all sides and in both scans in order to avoid uncertainties related to the differences in data acquisition methodology followed in the 2015 and 2018 campaigns (described in Section 2.3.1). In order to evaluate the completeness of point cloud coverage we applied a tree crown voxelization. The point clouds of crowns of all trees

for both years were voxelized using "VoxR" package (Lecigne et al., 2017). We applied a voxel size of 5 cm to capture even the small gaps and calculated the number of voxels for 2015 and 2018 for each tree. We estimated the percentage of change in the number of voxels between years. Taking into account the slow growth of holm oak we decided to retain for further analysis the trees with a change in number of voxels below 15%. This threshold was chosen after visual analysis of a variety of different thresholds. The total number of selected trees was n = 174: 42 for CT_P plot, 30 for CT_nP plot, 59 for NT plot, and 43 for ST plot (Fig. A2 in appendix).

2.6. Estimation of holm oak structural parameters using terrestrial laser scanning data

2.6.1. Estimation of the diameter at breast height

We developed two methods to estimate the DBH using TLS point clouds: the circumference method (CM) and the perpendiculars method (PM), which are based on the delineation of tree stem slices. Then, we compared the estimates of the two methods with that of a widely used circle-based fitting method (Fig. 2). Both the CM and circle fitting methods are based on the simplification that tree stem can be aligned with a ring shape (Olofsson et al., 2014; de Conto, 2019). We selected 36 tree stems that were sampled accurately with the TLS in 2015 (Fig. A2 in appendix) and isolated them from the denoized and normalized point cloud using the shapefile derived from the interpolated CHM. The CM and PM of the point clouds of each tree were sliced at 1.25–1.35 m vertically above the lowest point in the file (Fig. 2a).

The LAStools "*lasboundary*" tool was used to delineate the 2D projections of tree slices resulting in a ring-shaped polygon for each slice (Fig. 2b). The shapefiles were processed using SAGA GIS (Conrad et al., 2015). The TLS points of the tree slices were projected onto a 2D horizontal surface to obtain a closed ring boundary of stem slice, and the height for diameter acquisition was located in the middle of the slice. We generated two polygons for every slice: the "interior," from the hole, and the "exterior," from the polygon boundary, and we smoothed them using Gaussian smoothing for better fitting of the actual stem slice form. We assumed that the location of the stem boundary was between the "interior" hole and the "exterior" polygon boundary (Fig. 2b).

The DBH calculation followed field instrumental measurement protocols that are typically used for forestry inventories. The CM is based on the calculation of the DBH using the average of the perimeters of the "interior" and "exterior" polygons divided by π (Fig. 2c left). This method follows the same assumptions as estimating the diameter by measuring the circumference of a stem using a tape. On the other hand, the PM follows the caliper measurement technique: we generated 10 random perpendiculars passing through the centroid of each polygon of both "interior" and "exterior" using the R package "geosphere" (Hijmans, 2016). Then, we estimated the diameter as an average of the lengths of the perpendiculars (Fig. 2c right).

We used the random sample consensus (RANSAC) algorithm R package "TreeLS" (de Conto, 2019) to estimate the DBH using circle fitting. The points in the denoized and normalized point clouds of trees were classified to stem points using the "stemPoints" function of the package "TreeLS." The function was used to divide the tree stems vertically into several segments of 0.1 m of length, and it applied the Hough Transform shape detection algorithm to each segment to search the circles. If the segments matched the circle pattern, then the points were considered stem points. Then, the RANSAC algorithm was used to fit the circle to the classified stem points of the segments using the "stemSegmentation" function. The RANSAC algorithm was used to fit a circle to a subset of 20 points in the stem segment, and the fitting was repeated until the best fit was chosen. The DBH was calculated as an average value between 2 diameters located closest to 1.30 m. We implemented the RANSAC circle fitting 10 times and recorded the average diameter value for each tree to account for the RANSAC algorithm randomly choosing the points to fit the circle.

2.6.2. Estimation of the maximum tree height and crown projected area

Tree crowns were delineated following Chen et al. (2006). The value of each pixel of a binary image was replaced with the distance to its nearest nonzero pixel using a distance transformed image. The binary image was the interpolated CHM, where all the background pixels were masked with the value of one, and the tree cover pixels were represented with a no data value. Pixels with large distance values inside of the tree cover on the distance transformed image present the treetops. A watershed algorithm was applied to the inverted-distance transformed image to segment the tree crowns. The watershed algorithm represents each image as a landscape with segments as catchment basins and a segment boundary as a watershed line. The inverted-distance transformed image provides treetops as a local minimum for the watershed algorithm to start the segmentation process (Chen et al., 2006). All calculations were implemented using SAGA GIS (Conrad et al., 2015). The output of the delineation process was a shapefile, which represented each tree crown as an individual spatial polygon. However, some issues were visually detected in this shapefile: over-segmentation of some tree crowns if there were more than two primary branches, tree crowns segmented as two single trees, and under-segmentation of some trees when the trees had similar heights in areas with high tree densities, resulting in them being delineated as single trees. Over- and under-segmented tree crowns were manually corrected using QGIS software (QGIS Development Team, 2019).

After the segmentation process, each tree crown polygon was assigned an identifier (ID), and the respective coordinate of the crown centroid and the CA of each tree crown polygon were calculated. The h_{max} was calculated using the standard CHM as the maximum pixel (height) value inside each tree crown polygon. Field-measured DBH_f was assigned to the respective tree to analyze the biometric relationships further. For the trees without field measurements, DBH was calculated from TLS scans using the circumference method CM (DBH_{TLS}). We calculated the number of trees in 50 m diameter circles centered on every tree to obtain the local tree density (TD) for the biometric relationships.

2.7. Analysis of changes in tree structural parameters among different treatments, the relationship between changes

For the temporal analysis, we calculated the percentage change in h_{max} (Δh_{max}) and CA (ΔCA) for each selected tree using the following equations:

$$\Delta h_{max} = \frac{h_{max}2018 - h_{max}2015}{h_{max}2015} * 100\% \quad (1)$$

$$\Delta CA = \frac{CA2018 - CA2015}{CA2015} * 100\% \quad (2)$$

We selected the 16 trees equipped with dendrometers that matched with the respective trees in the point clouds of the two TLS scans to determine the relationships between changes in DBH and ΔCA and Δh_{max}. We used an absolute change in diameter between August 2015 and October 2018 to calculate percentage changes in DBH_d (ΔDBH_d):

$$\Delta DBH_d = \frac{DBH_d2018 - DBH_d2015}{DBH_d2015} * 100\% \quad (3)$$

The dataset of the structural properties derived as described in the Sections 2.6 and 2.7 are available in Bogdanovich et al. (2020).

2.8. Statistical analysis

All statistical analyses were implemented in R 3.4.1 (R Development Core Team, 2017). Linear regression analysis of the TLS-derived and orthophotograph-derived CA, as well as the TLS-derived and field-measured DBH was performed using least-square regressions. Pearson's correlation coefficient was also calculated.

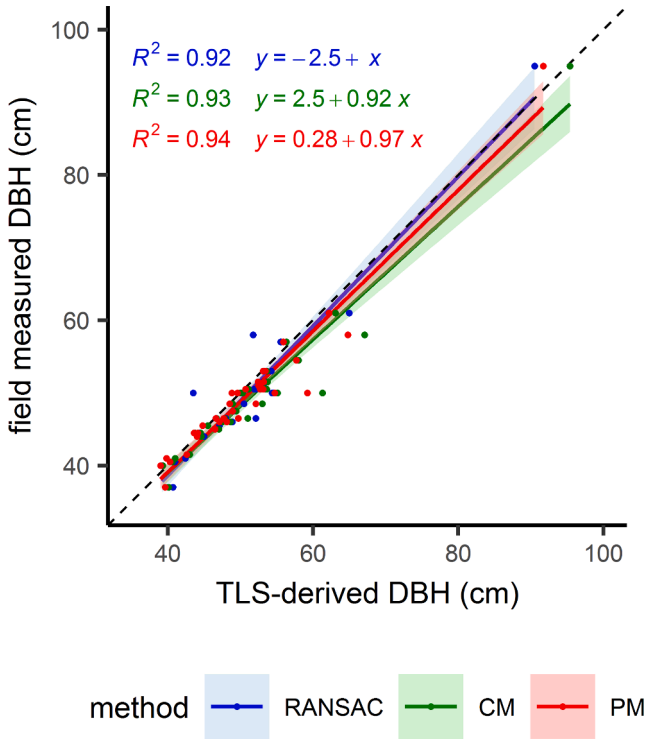

Fig. 3. Comparison between field-measured and TLS-derived DBH. Different colors represent different methods (CM – green color, PM – red color, RANSAC – blue color). CM method RMSE = 3.2 cm, MAE = 2.0 cm; PM method RMSE = 2.6 cm, MAE = 1.8 cm, RANSAC method RMSE = 2.8, MAE = 2.2. n = 36. The colored area represents the 95% confidence interval (CM – light green color, PM – light red color, RANSAC – light blue color). The dashed line is 1:1 line. (For interpretation of the references to color in this figure legend, the reader is referred to the web version of this article).

The errors of the estimated tree structural parameters were calculated using the root mean square error (RMSE) and mean absolute error (MAE) using Eq. (4) and Eq. (5), respectively:

$$RMSE = \sqrt{\frac{1}{n}\sum_{i=1}^{n}\left(y_i - \widehat{y}_i\right)^2} \quad (4)$$

$$MAE = \frac{1}{n}\sum_{i=1}^{n}\left|y_i - \widehat{y}_i\right| \quad (5)$$

where n is the number of observations, y_i is the TLS-estimated value, and $\widehat{y}_i$ is the measured value.

We conducted residual analysis, where the residuals of DBH obtained using the PM were plotted against the standard deviation of 10 perpendicular diameters. We applied the Shapiro-Wilk normality test ($p > 0.05$) to check the normality of the distribution of tree parameters for different treatments. We used Levene's test to check the homogeneity of variance. Tukey's honest significant difference (HSD) test was used to evaluate the significant differences in the tree structural parameters between different treatments. We used correlation analysis to determine how tree structural parameters relate to each other, in terms of the Pearson's correlation coefficient. We tested correlations between variables and the level of significance. The level of correlation significance was estimated using a *t*-test. Regression analysis was performed using least-square regressions. We used a Wilcoxon test to compare the medians of Δh_{max} and ΔCA between plots under the impact of different treatments and pruning because the distribution of the parameters was not normal.

3. Results

3.1. Estimation of holm oak structural parameters using terrestrial laser scanning data

Fig. 3 shows the relationship between the TLS-derived and field-measured DBH. Validation against field measurements indicated a good performance for all methods. The developed methods, as well as the RANSAC method, showed accuracy in diameter prediction. The CM showed $R^2 = 0.93$ (RMSE = 3.2 cm, MAE = 2.0 cm), the PM showed $R^2 = 0.94$ (RMSE = 2.6 cm, MAE = 1.8 cm), and the R^2 value for the RANSAC method was 0.92 (RMSE = 2.8 cm, MAE = 2.2 cm).

The residual analysis revealed that the sampled trees with the largest discrepancies were associated with the degree of asymmetry of their rings (Fig. 4a). Notably, the degree of asymmetry was defined here by the variance of the computed perpendicular diameters, as illustrated by the boxplot, resulting from a set of ring shapes in Fig. 4b–c. Based on visual inspection, the sampled trees with the largest discrepancies, such as ii-iv, Fig. 4a, belong to the tree stem slices with the highest standard deviation of perpendicular diameters (i.e., they have a more oval shape, Fig. 4b). As an illustrative example, Fig. 4b includes the extracted shapes of five stem slices, four of which represent the highest residuals (i–iv), and one represents the vast number with the lowest residual values (v). The shape of the slices with the tree identification "i-iv" are characterized as irregular, while the slice with identification "v" is characterized as regular (circular). A comparison of the variation of 10 perpendicular diameters for the selected slices shows that the diameter variation for irregular shapes is significantly higher than that representing regular shapes, which suggests that the observed bias is associated with asymmetric issues (Fig. 4c).

We compared TLS-derived CA in 2015 to orthophotograph-derived CA for 36 trees. Linear regression analysis showed that the TLS-derived CA agreed with the orthophotograph-derived CA (Fig. 5). The R^2 value was 0.86, and the RMSE was 15.74 m^2.

3.2. Characterization of the maximum tree height and crown area for the different treatments

First, we confirmed that the data are normally distributed (Shapiro-Wilk normality test $p > 0.05$). In addition, Levene's test confirmed the homogeneity of variance for all data ($p > 0.1$). The pruned trees (CT_P plot) had a significantly smaller CA (Tukey HSD, $p < 0.05$) in comparison with the control trees (CT_nP plot; Table 1) in 2015 and 2018. In 2015, CA in the CT_P plot was 89.36 ± 29.94 m^2 (μ +/− σ), and in the CT_nP, it was 108.31 ± 34.51 m^2.

In 2018, CA in the CT_P plot was 94.68 ± 32.65 m^2, and in the CT_nP, it was 112.34 ± 36.27 m^2. The differences in h_{max} between CT_P and CT_nP were also significant in both years (Tukey HSD, $p < 0.001$). The h_{max} in the CT_P plot was 7.86 ± 1.20 m, while in the CT_nP plot, it was almost 1 m higher (8.85 ± 1.03 m) in 2015. In 2018, h_{max} in the CT_P plot was 8.03 ± 1.25 m, while in the CT_nP plot it was 8.93 ± 1.05 m. For CT_P, NT, and NPT, the mean values of h_{max} and mean values of CA were not significantly different from each other (Tukey HSD, $p > 0.1$) in both years. The averaged DBHs were also similar for all plots (Tukey HSD, $p > 0.1$).

3.3. Biometric relationships between tree structural parameters

A statistically significant correlation was found between tree structural parameters (CA, h_{max}, and DBH) and TD for the selected trees in 2015 and 2018 ($p < 0.001$, Fig. 6).

Thus, significant positive correlations were found between CA and hmax in 2015 (R = 0.65) and 2018 (R = 0.67), and between h_{max} and DBH (R = 0.65) in 2015. The DBH was positively correlated with CA (R = 0.73) in 2015. Correlations between TD and CA and TD and h_{max} were significantly negative both in 2015 (R = −0.35) and 2018 (R = −0.36)

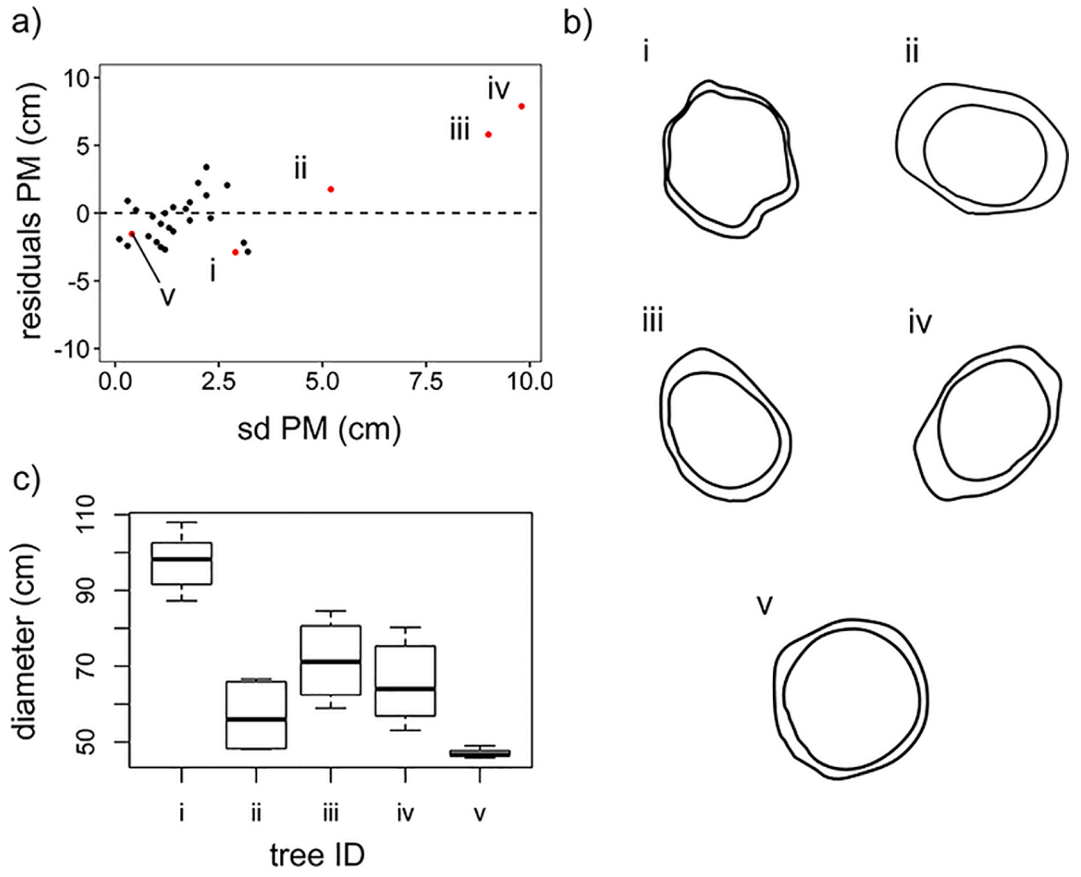

Fig. 4. Tree diameter residuals and tree slice shapes. (a) Scatter plot between residuals of DBH_{TLS}, obtained using PM method and standard deviation of the 10 perpendicular diameters that were taken for each tree slice. Chosen trees are colored in red and labeled by tree ID; (b) shapes of stem slices of selected trees; (c) comparison of distribution of 10 perpendicular diameters for the selected slices. (For interpretation of the references to color in this figure legend, the reader is referred to the web version of this article).

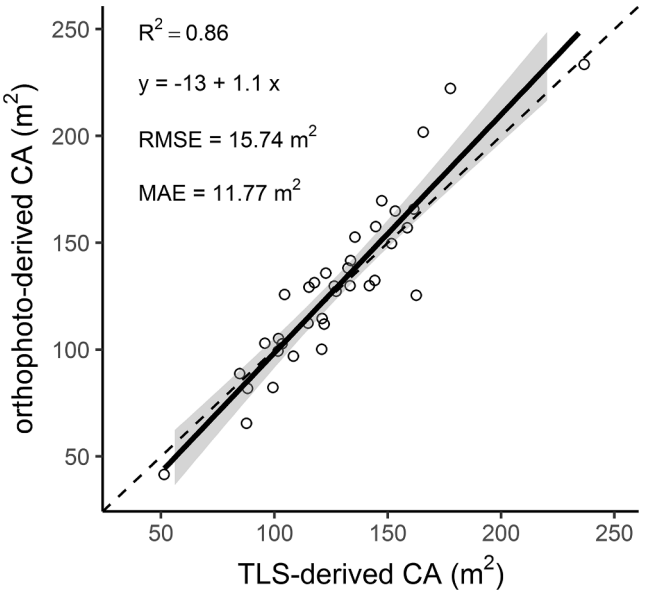

Fig. 5. Comparison between orthophotograph-derived CA and TLS-derived CA in 2015. The black line represents the linear regression between orthophotograph-derived CA and TLS-derived CA. The grey colored area represents the 95% confidence interval. The dashed line is 1:1 line. n = 36.

between TD and CA. Similarly, negative correlations were also found between TD and h_{max} in 2015 (R = −0.33) and 2018 (R = −0.35). In addition, TD was negatively correlated to DBH (R = −0.47) in 2015.

3.4. Analysis of changes in tree structural parameters among different treatments, the relationship between changes

We used a Wilcoxon test to compare the differences in ΔCA and Δh_{max} between plots under different treatments and pruning (Table 2). The median value of ΔCA for pruned trees (CT_P) was about 1.91% higher than the medians of ΔCA for control trees. According to the Wilcoxon test (Table 3), this difference was significant ($p < 0.01$). The medians of ΔCA for fertilized trees were similar, and the difference between them was not significant. There was a significant difference in the median values of Δh_{max} between the fertilized and control unpruned trees ($p < 0.01$ for CT_nP – NPT, $p < 0.001$ for CT_nP – NT). The smallest difference in Δh_{max} was observed for the control, unpruned trees (0.96 ± 1.60%). The difference in the median values of Δh_{max} between pruned and control trees was significant ($p < 0.01$). There was no significant difference in the median values of Δh_{max} between fertilized trees.

We compared changes in the DBH_d with the changes in CA and h_{max} for the 16 trees using dendrometers (Fig. 7). The highest significant correlation was found between ΔCA and Δh_{max} (R = 0.78). Significant correlations were found between ΔCA and Δh_{max} (R = 0.58) and between Δh_{max} and ΔDBH_d (R = 0.51).

Table 1
TLS-derived and measured tree parameters for each plot and year. CT_nP – control trees, CT_P – pruned trees, NT – nitrogen adding treatment, NPT – nitrogen and phosphorus adding treatment. Crown projected area (CA) and tree maximum height (h_{max}) are TLS-derived. n is number of trees for each plot. DBH_f is diameter at breast height measured in the field. For the trees without field measurements DBH was calculated from TLS using CM (DBH_{TLS}).

	2015				2018			
	CT_nP	CT_P	NT	NTP	CT_nP	CT_P	NT	NTP
Number of trees	n = 30	n = 42	n = 59	n = 43	n = 30	n = 42	n = 59	n = 43
CA (m^2)								
min	47.91	34.19	72.13	25.17	50.01	37.32	75.60	26.78
max	174.5	154.9	213.1	163.3	184.9	165.2	217.0	167.0
mean ± sd	108.31 ± 34.51	89.36 ± 29.94	118.46 ± 32.12	104.48 ± 29.89	112.34 ± 36.27	94.68 ± 32.65	122.79 ± 33.25	107.48 ± 30.63
h_{max} (m)								
min	7.23	5.41	6.52	5.90	7.25	5.55	6.59	6.00
max	11.12	10.90	12.53	10.63	11.20	11.13	13.30	10.69
mean ± sd	8.85 ± 1.03	7.86 ± 1.20	8.79 ± 1.14	9.09 ± 1.06	8.93 ± 1.05	8.03 ± 1.25	8.98 ± 1.20	9.24 ± 1.08
DBH (cm)Number of trees DBH_f /DBH_{TLS}	n = 24/6	n = 42/0	n = 59/0	n = 37/6	No measurements			
min	34.0	31.0	31.5	21.0				
max	63.5	62.5	67.0	62.5				
mean ± sd	46.4 ± 6.7	45.7 ± 7.2	48.7 ± 7.5	46.9 ± 8.4				

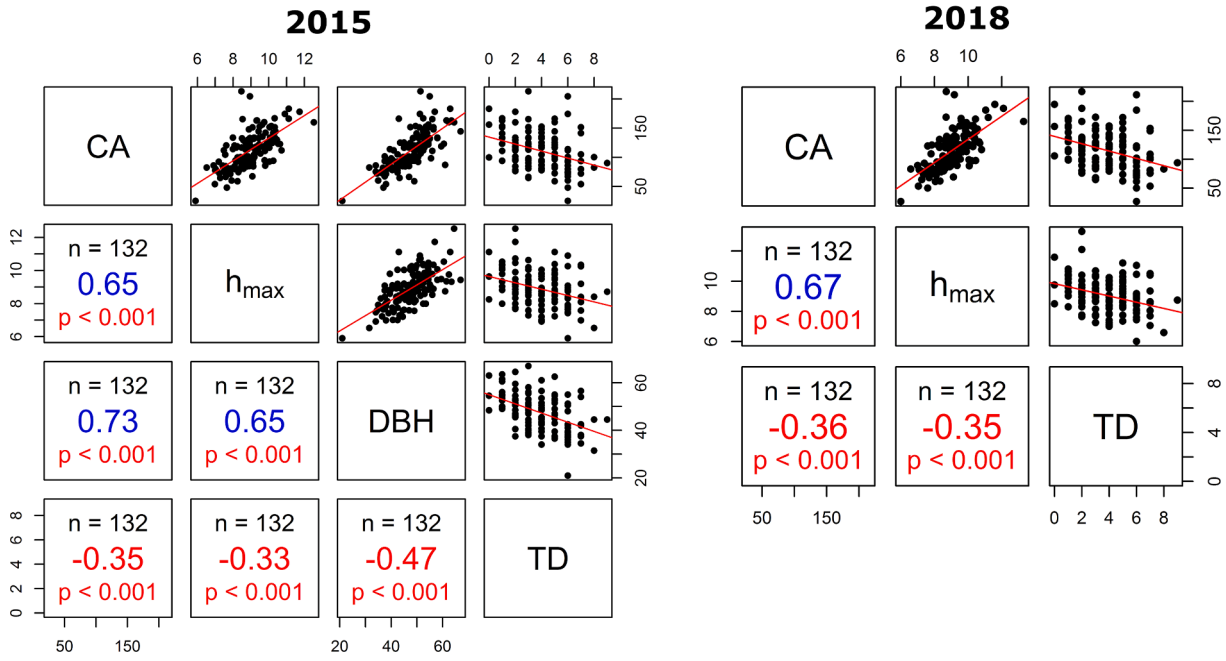

Fig. 6. Correlation matrix of average values of CA (m^2), h_{max} (m), DBH (cm), and TD. 2015 is on the left matrix, 2018 is on the right one. All treatments are included except pruned trees. DBH included field measured DBH and TLS-derived DBH (for the trees without field measurements DBH was calculated from TLS scans using CM). There are no DBH measurements for 2018. Upper right boxes display the scatterplots and a linear square fit of the variables (red line). Lower left boxes show level of significance (p), the Pearson's correlation coefficient (in the middle) and number of samples (n). The diagonal boxes show the variables. Positive correlation coefficient is colored in blue, negative correlation coefficient is colored in red. Level of significance <0.05 is colored in red. (For interpretation of the references to color in this figure legend, the reader is referred to the web version of this article).

Table 2
Comparison of percentage changes in tree parameters between different treatments and pruning.

	Number of trees	Median ± interquartile range		
Plots		**ΔCA (%)**	**Δh_{max} (%)**	**Δh_{max} /ΔCA**
CT_P	42	5.63 ± 3.80	1.92 ± 2.24	0.36 ± 0.53
CT_nP	30	3.71 ± 2.77	0.96 ± 1.60	0.22 ± 0.46
NT	59	3.59 ± 2.96	2.02 ± 1.91	0.57 ± 0.58
NPT	43	3.25 ± 2.71	1.66 ± 1.37	0.55 ± 0.68

4. Discussion

4.1. Estimation of tree structural parameters and validation against field measurements

Our results show that TLS can be used to retrieve data on the dynamic changes in state variables of vegetation as defined by tree key structural parameters, CA, h_{max}, and DBH, in open woodlands.

Diameter calculations assume a circular form of the cross-section that is not necessarily common in nature. Deformations of tree stem are associated with environmental conditions, such as wind, mechanical damage, including pruning, and the influence of pathogens (Wade and Hewson, 1979; Mattheck, 1998; Mattheck and Tesari, 2004; Pulkkinen, 2012). TLS allows capturing the structural features of tree stem and

Table 3
Results of Wilcoxon test. Bold values denote statistical significance at the $p < 0.05$ level. W is the Wilcoxon test statistic.

	ΔCA (%)				Δh_{max} (%)			
			95% Confidence interval				95% Confidence interval	
Plots	p-value	W	Lower	Upper	p-value	W	Lower	Upper
CT_P – CT_nP	**<0.01**	897.5	0.66	3.30	**<0.01**	869.0	0.33	1.89
CT_nP – NPT	0.170	768.0	−0.33	1.60	**<0.01**	381.5	−1.38	−0.24
CT_nP – NT	0.952	892.5	−0.86	0.99	**<0.001**	450.5	−1.75	−0.54
NT – NPT	0.162	1061.5	−1.45	0.20	0.186	1073.0	−0.87	0.13

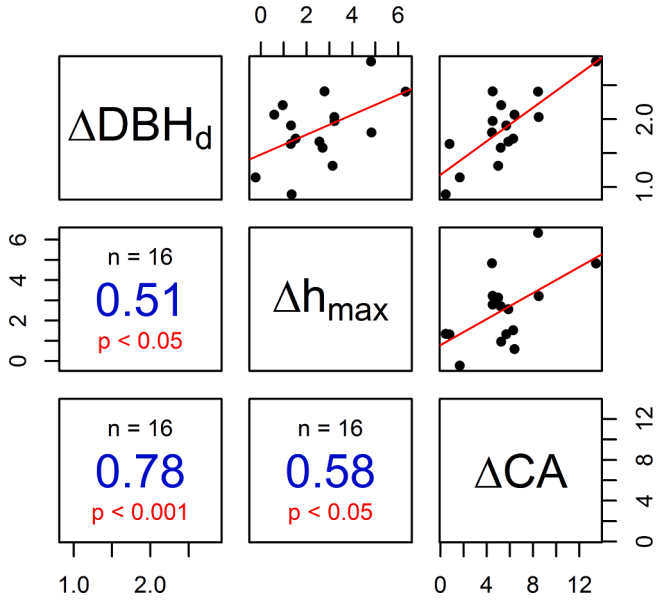

Fig. 7. Correlation matrix of ΔDBH_d (%), Δh_{max} (%) and ΔCA (%). Upper right boxes display the scatterplots and a linear square fit of the variables (red line). Lower left boxes show significant level (p), the Pearson's correlation coefficient (in the middle) and number of trees (n). The diagonal boxes show the variables. Positive correlation coefficient is colored in blue. Level of significance <0.05 is colored in red. (For interpretation of the references to color in this figure legend, the reader is referred to the web version of this article).

estimate DBH with high accuracy. The degree of stem asymmetry is a source of uncertainty underpinning field measurements of DBH using calipers or measuring tapes. Similar sources of errors are reported for the use of cylinder or circle fitting methods (Moskal and Zheng, 2011; Srinivasan et al., 2015) to calculate diameters using TLS.

Here we further developed point cloud slice-based methods to estimate DBH of holm oak trees in a Mediterranean open woodland using the TLS scans. Both of our calculation methods, PM and CM, showed close agreement with field measurements. The methods are also comparable to the widely used RANSAC algorithm. In particular, PM improved the accuracy (i.e., lower RMSE and MAE) compared with CM and RANSAC. Our results suggest that the source of uncertainties was primarily associated with irregular (non-circular) shapes of stem slices. The tree "i" in our study (Fig. 4) is an example of a non-regular cross-section. The PM takes into account the asymmetry of stem cross-section of holm oak. We showed that the shape factor could be more accurately evaluated using the standard deviation of the averaged length of random perpendicular diameters: regular-formed slice shapes had the lowest standard deviations, indicating more accuracy because the lengths of the perpendicular diameters were almost equal. At the same time, irregularly shaped slices showed relatively high standard deviations, indicating less accuracy (Fig. 4). TLS point clouds of trees were sliced parallel to the ground, while the cross-section of trees, including those that were tilted, were taken during field measurements perpendicular to the longitudinal axis of the stem, regardless of stem inclination. This approach can lead to a misrepresentation of cross-section shapes, e.g. an elliptical shape for a circular stem cross-section for a non-vertical tree. This problem could be solved by rotating the point cloud of each tree to account for the inclination angle. However, this procedure requires longer computational processing, especially when there are numerous tree counts.

In terms of the density of point cloud and slice thickness, based on visual inspections of the point cloud, we can conclude that some trees had a heterogeneous density along the slices with more points on one side and less on the opposite side to the angles of the scans due to TLS occlusions. Although an optimal number of scan positions would always reduce this issue, the occlusion problem could be solved by increasing slice thickness. Slice thickness does not affect trees with straight stems, but in the case of tilted stems, it might be a prominent source of error. For instance, we found diameter errors of up to 8 cm, which can lead to significant miscalculations of whole-plant variables, such as stem biomass, and it might affect other biometric relations, such as DBH and h_{max}. Therefore, our results demonstrated that accounting for this effect provides a more accurate estimation than standard approaches, particularly for stands with irregular shapes.

The comparison with CA derived from orthophotographs demonstrated the potential of TLS to derive metrics related to crown areas, especially for trees with complex crown structures, such as the holm oak. Popescu and Zhao (2008) showed an R^2 value of 0.59 for crown width estimation with ALS for deciduous trees, while (Srinivasan et al., 2015) reported R^2 values of 0.84 with TLS. Our results showed correlations of up to 0.86, which is close to the range of other LiDAR studies. For the estimation of the crown area of trees in Mediterranean woodland ecosystems, orthophotographs are best utilized during the dry season, when there is a substantial contrast in the reflectance between the trees and understory (Carreiras et al., 2006). Despite the relatively high spectral contrast between the trees and the dry grass understory in the orthophotograph used in this study, the similar spectral values of the tree foliage and canopy shadows complicated the delineation of crowns and may have been a potential source of error. Whereas the orthophotograph method relies on spectral differentiation, TLS is a direct physical measure of structure. As demonstrated in this study where TLS surveys from dry and wet seasons were used, TLS is suitable for this purpose independent of the season. Additionally, the raster CHM derived from the TLS had a higher spatial resolution than the orthophotographs: 0.05 m compared with 0.25 m, respectively. It should be noted that one source of uncertainty in our results is the difference in the years of acquisition for TLS and the orthophotographs: orthophotograph was taken in 2016, while the TLS data were from 2015 and 2018.

TLS can also be used to calibrate allometric relationships, such as DBH and h_{max} at the tree level (Sun et al., 2016; Lau et al., 2019), for modeling purposes (Raumonen et al., 2013; Hackenberg et al., 2014), and the estimation of biomass stocks at the ecosystem level (Calders et al., 2015; Stovall et al., 2017).

The application of TLS for structural measurement of open woodlands was not without some limitations. As reported in the literature, the accuracy of the retrieval of canopy metrics using TLS is influenced by the degree of occlusion, which can often lead to underestimation of tree height (Hopkinson et al., 2004; Moskal and Zheng, 2011; Olofsson et al.,

2014; Srinivasan et al., 2015). However, the low tree density of open woodlands enabled the more accurate delineation of trees in comparison with dense boreal or temperate stands. Nevertheless, even in open woodlands, we showed that occlusion can be a problem, and for this reason, we excluded some trees from the study. Occlusion occurred primarily in areas where the distribution of trees was denser. An increase in the number of scanning locations in those areas would help to alleviate this problem (Srinivasan et al., 2015; Sheppard et al., 2016). The second TLS acquisition in this study in 2018 was conducted with a higher number of scanning locations, which resulted in more comprehensive coverage of scanned objects. The relatively flat crowns of holm oaks complicated tree delineation because the top of the crown is often naturally misplaced from the center point due to the growth of trees. Chen et al. (2006) reported overestimation for trees with large crowns and underestimation for overlapped crowns of neighbor trees. Furthermore, noise in the data at the edge of crowns due to wind effects during TLS data acquisition may have an influence on accurate tree delineation and, therefore, height and canopy area estimation (Dassot et al., 2011).

4.2. Biometric relationships between tree structural parameters

In this study, we characterize the variability of TLS-derived biometric relationships between three key state variables of holm oak trees in Mediterranean open woodland: maximum tree height (h_{max}), crown projected area (CA), and DBH. Overall, we found a significant correlation between the three tree structural parameters, CA, DBH, h_{max}, and site-level properties, such as TD, which were derived from field observations and TLS. Correlation values were similar in different years. Considering that holm oak trees are anthropogenically shaped by periodical pruning (Joffre et al., 1999), the presence of a significant correlation between tree parameters is not usually found.

The strong correlation between DBH and other structural parameters (h_{max} and CA) means that higher trees with wider canopies have larger DBH. This is coherent with the positive association between the crown area and DBH shown by Verbeeck et al. (2019) over > 1000 trees. Diameter growth is an adaptive mechanism of trees to provide support to heavy crowns (McMahon, 1973). We also found a strong correlation between h_{max} and CA ($R = 0.65$, $p < 0.001$ in 2015). CA and h_{max} are not always related across different tree species (Jackson et al., 2019), but within holm oak, a positive relationship seems to exist. The positive correlation between tree height and canopy width ($R = 0.52$, $p < 0.001$) has been reported for holm oak by Pulido et al. (2001). At the same time, we found that DBH was more closely related to CA than to h_{max} ($R = 0.73$, $p < 0.001$ and 0.65, $p < 0.001$, respectively), which indicated the effect of pruning on the canopy shape. Pruning aims is to shape a wide tree canopy to maximize light interception and acorn production (Joffre et al., 1999).

Inter-specific variability of tree structural components can lead to uncertainties in biomass estimation if using biomass equations non-calibrated to a specific study site (Forrester et al., 2017). For instance, Pulido et al. (2001) found a weaker correlation between canopy width and DBH ($R = 0.63$, $p < 0.001$) for another *dehesa* study site. Our results can elucidate the relationship between key structural parameters in holm oak (Verbeeck et al., 2019).

We found a negative correlation between estimated tree structural parameters and TD, which may indicate the presence of intraspecific competition between the trees that can affect tree size (Thorpe et al., 2010; del Río et al., 2019). The sparse trees have more soil and water available, which allows them to avoid water stress and, therefore, survive during the drought (Moreno and Cubera, 2008). Gea-Izquierdo and Canellas (2009) demonstrated the negative effect of intraspecific competition on holm oak growth using a regression model, although they concluded that tree age more likely impacted tree growth. Interestingly, we found that tree density fitted using the classical biometric relationship with DBH ($TD = 10^4$ ($DBH^{-1.6}$), for a mean DBH of 49 cm provided a TD of 19 tree ha^{-1}, which agreed with Reineke's rules (Reineke, 1933). Our results demonstrated the practical application of TLS in deriving key state variables and biometric constraints for dynamic vegetation modeling.

At the higher level of ecological integration, the relationship between DBH and canopy fraction cover is alternatively used for estimating stand-level transpiration. Perez-Priego et al. (2017) used DBH as a key plant trait for linking both whole-plant level and stand-level transpiration in the studied Mediterranean open woodland.

4.3. Analysis of changes in tree structural parameters

The two scans from 2015 and 2018 provided an accurate description of the influence of different management treatments on the growth rate of crown area and maximum tree height. We demonstrated that TLS measurements allow capturing even small changes in structural parameters, which is essential for such slow-growing species as holm oak. Furthermore, TLS was able to detect differences in the growth rate, which is the result of the impact of different treatments. Multitemporal TLS was able to inform the effect of different drivers, such as pruning and fertilization, on vegetation structure dynamics. This finding supports the idea that proximal and remote sensing are valuable tools for understanding the dynamics and structure of ecosystems in research stations (Shiklomanov et al., 2019).

We found that lateral growth prevails for all trees. This finding was also confirmed by the correlation analysis of changes in structural parameters. In particular, ΔDBH_d was more correlated with ΔCA than Δh_{max} that indicates the effect of pruning on canopy shape. Pruning aims to shape a wide tree canopy to maximize light interception and acorn production (Joffre et al., 1999). The correlation performed better if the acquisition dates for the different parameters were the same. Changes in DBH are difficult to measure for slow-growing trees, such as holm oaks: the mean value of ΔDBH_d was only 0.30 cm/year. Changes in diameter may also relate to tree age (Gea-Izquierdo et al., 2008), tree health (Solla et al., 2009; Corcobado et al., 2014) or climate conditions (Gutiérrez et al., 2011).

Despite pruning being the most popular treatment (Plieninger et al., 2004), there is a lack of research on canopy recovery and canopy growth rates after pruning. Our results showed that pruning had more effects on lateral growth compared with nutrient fertilization treatments. This finding is related to the canopy recovery processes after pruning, which increase the number of yearly shoots per brunch (Marini, 2009).

Our results showed that the fertilized trees grew more in height than the non-fertilized ones, which is in agreement with other nutrient-related studies focused on characterizing the effect of fertilization on the growth of holm oak trees. For instance, Pulido et al. (2013) showed that the addition of nitrogen, phosphorus, and potassium (NPK) resulted in the production of longer shoots in the tree canopy. Rivest et al. (2011) showed that tree growth (annual shoot elongation) was affected positively by fertilization, especially by nitrogen fertilization. However, stem diameter growth did not respond to phosphorus or nitrogen soil fertilization (Mayor and Rodà, 1994; Martin et al., 2015). Mayor and Rodà (1994) suggested that the trees preferably used the nutrients for canopy foliage production.

The use of LiDAR to detect dynamic changes in vegetation has some limitations that need to be considered. As reported by other studies focused on estimating changes in tree structural parameters using LiDAR time series, one major problem is the precise alignment of tree point clouds and repeatable parameter estimations despite variations in LiDAR acquisitions (Hopkinson et al., 2004; Duncanson and Dubayah, 2018). Occluded areas complicate the precise estimation of tree parameters (Hopkinson et al., 2004; Moskal and Zheng, 2011; Olofsson et al., 2014; Srinivasan et al., 2015), but increasing the density of scanning locations helps to avoid this problem (Sheppard et al., 2016). In our study, the different number of scan locations in the two sampling years resulted in different point cloud densities and the illumination of the tree canopies. This complicated the estimation of changes because it

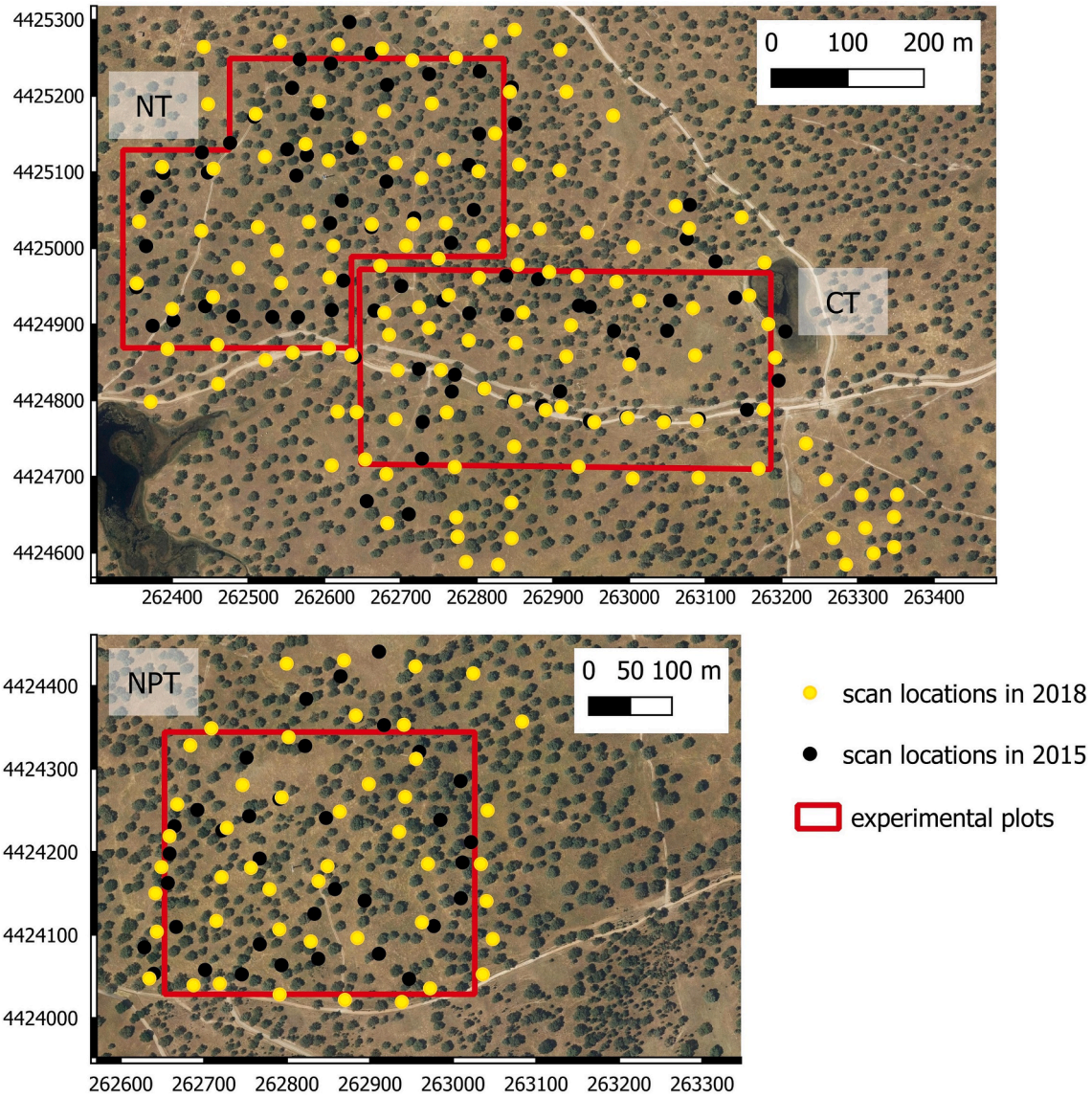

Fig. A1. Orthophotograph in UTM projection with scan locations, selected for this study in 2015 and 2018. CT_nP - control treatment (no fertilization, no pruning), CT_P – pruned area, NT – nitrogen added treatment, NPT – nitrogen and phosphorus added treatment. The true-color RGB orthophotograph was provided by the Spanish National Orthophotography Program (PNOA in Spanish) database. (For interpretation of the references to color in this figure legend, the reader is referred to the web version of this article).

is difficult to determine whether there is significant shoot growth or one side of the tree canopy is poorly sampled by the TLS. Even for an ecosystem with such a low tree density, the study requires appropriate filtering of trees whose scans are suitable for the detection of such change. In addition, remote sensing data or previous information on the mapping of crowns in the study site might be used to optimize sampling locations in TLS campaigns. Visual analyses could contribute to determine the locations that maximize data density for a limited number of TLS locations.

5. Conclusions

TLS showed good performance in the retrieval of the three measured structural parameters of vegetation, DBH, CA, and h_{max}, and their biometric relationships in a heterogeneous Mediterranean woodland characterized by sparse trees.

We developed two TLS-based DBH calculation methods. Both methods accurately matched field observations ($R^2 = 0.93–0.94$, RMSE = 2.61–3.2 cm) and outperformed standard approaches. In particular, we showed that factors, such as a tree inclination, which led to asymmetrical shapes of the slices, and a low point density of the TLS point cloud are prominent sources of uncertainties. For instance, the irregular shape of a cut led to residuals of up to 8 cm, which had substantial implications for whole-plant accounting when it might cause errors in biomass calculation. The proposed approach can be further improved using geometrical functions to reduce the uncertainty related to tree inclination.

TLS accurately estimated tree CA. Inter-comparison with orthophoto-derived CA showed an R^2 value of 0.86, and RMSE was 15.74 m^2. The approach can also be used to calibrate allometric relationships, such as DBH and h_{max}, at the tree level (Sun et al., 2016; Lau et al., 2019), for modeling purposes (Raumonen et al., 2013; Hackenberg et al., 2014), and estimate biomass stocks at the ecosystem level (Calders et al., 2015; Stovall et al., 2017). Moreover, TLS enabled the characterization of how biometric relations were shaped by vital site-level properties, such as tree density.

Our case study illustrates several ecological applications of TLS despite the challenges of discerning precise dynamic changes for slow-

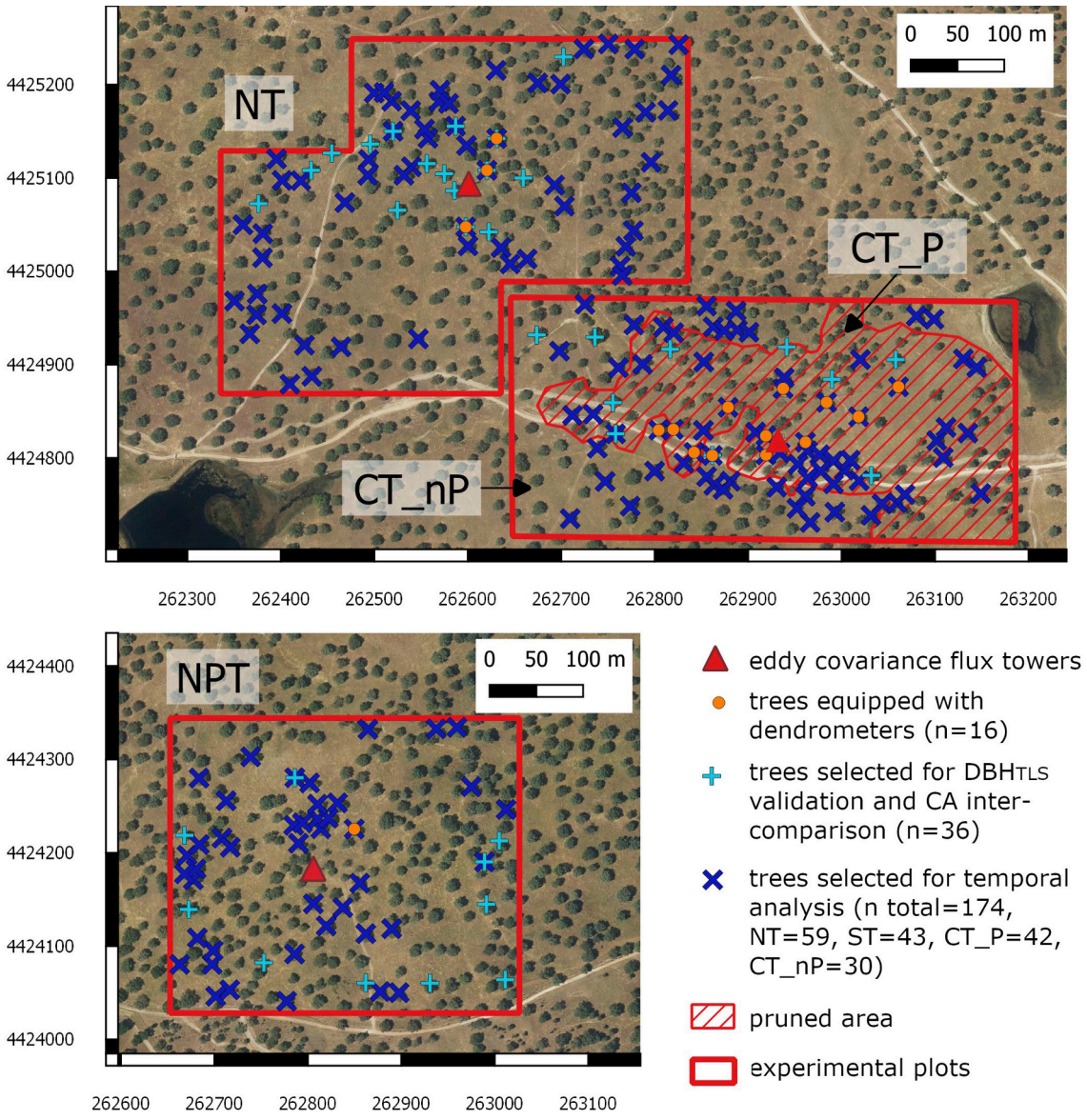

Fig. A2. Orthophotograph in UTM projection with locations of trees, selected for this study. CT_nP - control treatment (no fertilization, no pruning), CT_P – pruned area, NT – nitrogen added treatment, NPT – nitrogen and phosphorus added treatment. The true-color RGB orthophotograph was provided by the Spanish National Orthophotography Program (PNOA in Spanish) database. (For interpretation of the references to color in this figure legend, the reader is referred to the web version of this article).

growing trees, such as holm oak. Our multitemporal scanning provided an accurate description of the influence of different management treatments on changes in tree structural properties such as CA and h_{max}. In particular, we found that (i) lateral growth prevails for all trees, (ii) pruning has more substantial effects on lateral than vertical growth, whereas fertilized trees grow more in height (iii) and both nutrient fertilization and pruning affected biometric relationships among changes in tree structural properties.

Future work could expand our study area, using the same scan protocol for TLS. The various additional metrics related to tree crown (e.g. crown base height, bulk volume), branching (e.g. size, angle, and distribution), or/and foliage density (e.g. clumping index, gap distribution) should be estimated for full and more accurate analysis of tree growth. Integrating ALS or UAV LiDAR and TLS would reduce occlusions and improve the accuracy of the calculation of structural parameters. It would also be interesting to apply the developed methodology to time series.

CRediT authorship contribution statement

Ekaterina Bogdanovich: Methodology, Formal analysis, Data curation, Writing - original draft, Visualization. **Oscar Perez-Priego:** Conceptualization, Writing - review & editing, Supervision. **Tarek S. El-Madany:** Conceptualization, Resources, Writing - review & editing. **Marcus Guderle:** Conceptualization, Resources, Writing - review & editing. **Javier Pacheco-Labrador:** Resources, Writing - review & editing. **Shaun R. Levick:** Conceptualization, Writing - review & editing. **Gerardo Moreno:** Project administration, Writing - review & editing. **Arnaud Carrara:** Resources. **M. Pilar Martín:** Writing - review & editing, Project administration. **Mirco Migliavacca:** Conceptualization, Writing - review & editing, Project administration, Funding acquisition, Supervision.

Declaration of Competing Interest

The authors declare that they have no known competing financial

interests or personal relationships that could have appeared to influence the work reported in this paper.

Data availability

The data used for statistical analysis in this paper, as well as the structural properties of tree derived from TLS are available at the following link http://doi.org/10.5281/zenodo.3981011.

Acknowledgment

The authors acknowledge the Alexander von Humboldt Foundation and the Max Planck Research Prize 2013 to Markus Reichstein that funded the research. E.Bogdanovich, M.Migliavacca acknowledge the support of the Trustee European Commission project no H2020-MSCA-ITN-2016 – 721995. M. Migliavacca and J.Pacheco-Labrador acknowledge the DLR project OBEF-Accross2 "The Potential of Earth Observations to Capture Patterns of Biodiversity" (Contract No. 50EE1912, German Aerospace Center). The authors are grateful to the Spanish National Center of Geographical Information (CNIG) that provided the Orthophotographs used in the study.

Appendix

See Figs. A1 and A2.

References

Ahlström, A., Raupach, M.R., Schurgers, G., Smith, B., Arneth, A., Jung, M., Reichstein, M., Canadell, J.G., Friedlingstein, P., Jain, A.K., Kato, E., Poulter, B., Sitch, S., Stocker, B.D., Viovy, N., Wang, Y.P., Wiltshire, A., Zaehle, S., Zeng, N., 2015. The dominant role of semi-arid ecosystems in the trend and variability of the land CO2 sink. Science 348, 895–899.

Axelsson, P., 2000. DEM generation from laser scanner data using adaptive TIN models. XIXth ISPRS Congress Amsterdam 110–117.

Béland, M., Widlowski, J.-L., Fournier, R.A., Côté, J.-F., Verstraete, M.M., 2011. Estimating leaf area distribution in savanna trees from terrestrial LiDAR measurements. Agric. For. Meteorol. 151, 1252–1266.

Bienert, A., Hess, C., Maas, H.-G., von Oheimb, G., 2014. A voxel-based technique to estimate the volume of trees from terrestrial laser scanner data. ISPRS Archives 40, 101–106.

Bienert, A., Scheller, S., Keane, E., Mohan, F., Nugent, C., 2007. Tree detection and diameter estimations by analysis of forest terrestrial laserscanner point clouds. ISPRS Workshop on Laser Scanning 2007 and SilviLaser 2007, Espoo, Finland, pp. 50-55.

Bogdanovich, E., Perez-Priego, O., El-Madany, T.S., Guederle, M., Pacheco-Labrador, J., Levick, S.R., Moreno, G.M., Carrara, A., Martín, M. P., Migliavacca, M., 2020. Majadas de Tietar - Tree structural parameters from Terrestrial Lidar Scanning (2015, 2018) (Version 1.0) [Data Set]. http://doi.org/10.5281/zenodo.4501516.

Calders, K., Newnham, G., Burt, A., Murphy, S., Raumonen, P., Herold, M., Culvenor, D., Avitabile, V., Disney, M., Armston, J., Kaasalainen, M., 2015. Nondestructive estimates of above-ground biomass using terrestrial laser scanning. Methods Ecol. Evol. 6, 198–208.

Carreiras, J.M.B., Pereira, J.M.C., Pereira, J.S., 2006. Estimation of tree canopy cover in evergreen oak woodlands using remote sensing. For. Ecol. Manage. 223, 45–53.

Chave, J., Andalo, C., Brown, S., Cairns, M.A., Chambers, J.Q., Eamus, D., Fölster, H., Fromard, F., Higuchi, N., Kira, T., Lescure, J.-P., Nelson, B.W., Ogawa, H., Puig, H., Riéra, B., Yamakura, T., 2005. Tree allometry and improved estimation of carbon stocks and balance in tropical forests. Oecologia 145, 87–99.

Chen, Q., Baldocchi, D., Gong, P., Kelly, M., 2006. Isolating individual trees in a savanna woodland using small footprint lidar data. Photogramm. Eng. Remote Sens. 72, 923–932.

Cho, M.A., Mathieu, R., Asner, G.P., Naidoo, L., van Aardt, J., Ramoelo, A., Debba, P., Wessels, K., Main, R., Smit, I.P., Barend, E., 2012. Mapping tree species composition in South African savannas using an integrated airborne spectral and LiDAR system. Remote Sens. Environ. 125, 214–226.

Colgan, M.S., Baldeck, C.A., Féret, J.-B., Asner, G.P., 2012. Mapping savanna tree species at ecosystem scales using support vector machine classification and BRDF correction on airborne hyperspectral and LiDAR data. Remote Sens. 4, 3462–3480.

Conrad, O., Bechtel, B., Bock, M., Dietrich, H., Fischer, E., Gerlitz, L., Wehberg, J., Wichmann, V., Böhner, J., 2015. System for automated geoscientific analyses (SAGA) v. 2.1. 4. Geosci. Model Dev. 8, 1991–2007.

Corcobado, T., Cubera, E., Juárez, E., Moreno, G., Solla, A., 2014. Drought events determine performance of Quercus ilex seedlings and increase their susceptibility to Phytophthora cinnamomi. Agric. For. Meteorol 192, 1–8.

Dassot, M., Constant, T., Fournier, M., 2011. The use of terrestrial LiDAR technology in forest science: application fields, benefits and challenges. Ann. For. Sci. 68, 959–974.

de Conto, T., 2019. TreeLS: Terrestrial Point Cloud Processing of Forest Data. R package version 1.0.

del Río, M., Bravo-Oviedo, A., Ruiz-Peinado, R., Condés, S., 2019. Tree allometry variation in response to intra- and inter-specific competitions. Trees 33, 121–138.

Duncanson, L., Dubayah, R., 2018. Monitoring individual tree-based change with airborne lidar. Ecol. Evol. 8, 5079–5089.

El-Madany, T.S., Reichstein, M., Perez-Priego, O., Carrara, A., Moreno, G., Martín, M.P., Pacheco-Labrador, J., Wohlfahrt, G., Nieto, H., Weber, U., Kolle, O., Luo, Y.-P., Carvalhais, N., Migliavacca, M., 2018. Drivers of spatio-temporal variability of carbon dioxide and energy fluxes in a Mediterranean savanna ecosystem. Agric. For. Meteorol. 262, 258–278.

Forrester, D.I., Tachauer, I.H.H., Annighoefer, P., Barbeito, I., Pretzsch, H., Ruiz-Peinado, R., Stark, H., Vacchiano, G., Zlatanov, T., Chakraborty, T., 2017. Generalized biomass and leaf area allometric equations for European tree species incorporating stand structure, tree age and climate. For. Ecol. Manage. 396, 160–175.

García, M., Gajardo, J., Riaño, D., Zhao, K., Martín, P., Ustin, S., 2015. Canopy clumping appraisal using terrestrial and airborne laser scanning. Remote Sens. Environ. 161, 78–88.

Gea-Izquierdo, G., Canellas, I., 2009. Analysis of holm oak intraspecific competition using Gamma regression. For. Sci. 55, 310–322.

Gea-Izquierdo, G., Cañellas, I., Montero, G., 2008. Site index in agroforestry systems: age-dependent and age-independent dynamic diameter growth models for Quercus ilex in Iberian open oak woodlands. Can. J. For. Res. 38, 101–113.

Gutiérrez, E., Campelo, F., Camarero, J.J., Ribas, M., Muntán, E., Nabais, C., Freitas, H., 2011. Climate controls act at different scales on the seasonal pattern of Quercus ilex L. stem radial increments in NE Spain. Trees 25, 637–646.

Hackenberg, J., Morhart, C., Sheppard, J., Spiecker, H., Disney, M., 2014. Highly accurate tree models derived from terrestrial laser scan data: A method description. Forests 5, 1069–1105.

Hayat, A., Hacket-Pain, A.J., Pretzsch, H., Rademacher, T.T., Friend, A.D.J.F.i.p.s., 2017. Modeling tree growth taking into account carbon source and sink limitations. 8, 182.

Henry, M., Picard, N., Trotta, C., Manlay, R., Valentini, R., Bernoux, M., Saint-André, L., 2011. Estimating tree biomass of sub-Saharan African forests: a review of available allometric equations. Silva Fenn. 45, 477–569.

Herrero-Huerta, M., Lindenbergh, R., Rodríguez-Gonzálvez, P., 2018. Automatic tree parameter extraction by a Mobile LiDAR System in an urban context. PLoS ONE 13, e0196004.

Hijmans, R.J., 2016. Geosphere: Spherical Trigonometry. R package version 1.5-5. . https://CRAN.R-project.org/package=geosphere.

Hill, M.J., Hanan, N.P., Hoffmann, W., Scholes, R., Prince, S., Ferwerda, J., Lucas, R.M., Baker, I., Arneth, A., Higgins, S., Barrett, D.J., Disney, M., Hutley, L., 2011. Remote sensing and modeling of savannas: The state of the dis-union. Proceedings of the 34th International Symposium on Remote Sensing of the Environment (ISRSE), Sydney, NSW, Australia, pp. 10–15.

Hopkinson, C., Chasmer, L., Hall, R.J., 2008. The uncertainty in conifer plantation growth prediction from multi-temporal lidar datasets. Remote Sens. Environ. 112, 1168–1180.

Hopkinson, C., Chasmer, L., Young-Pow, C., Treitz, P., 2004. Assessing forest metrics with a ground-based scanning lidar. Can. J. For. Res. 34, 573–583.

Houghton, R.A., Hall, F., Goetz, S.J., 2009. Importance of biomass in the global carbon cycle. J. Geophys. Res. 114, G00E03.

Houghton, R.A., Lawrence, K.T., Hackler, J.L., Brown, S., 2001. The spatial distribution of forest biomass in the Brazilian Amazon: a comparison of estimates. Global Change Biol. 7, 731–746.

Huntsinger, L., Campos, P., Starrs, P.F., Oviedo, J.L., Díaz, M., Standiford, R.B., Montero, G., 2013. Working landscapes of the Spanish Dehesa and the California oak woodlands: an introduction. In: Campos, P., Huntsinger, L., Oviedo, J.L., Starrs, P.F., Díaz, M., Standiford, R.B., Montero, G. (Eds.), Mediterranean Oak Woodland Working Landscapes. Springer, Dordrecht, pp. 3–23.

Husch, B., Beers, T.W., Kershaw Jr, J.A., 2002. Forest Mensuration. John Wiley & Sons, Hoboken.

ICT international, DBL60 Stand-Alone Logging Dendrometer. http://www.ictinternational.com/pdf/?product_id=89. (accessed 23.06.2020).

Isenburg, M., 2014. Rasterizing Perfect Canopy Height Models from LiDAR. https://rapidlasso.com/2014/11/04/rasterizing-perfect-canopy-height-models-from-lidar/ (accessed 15.11.2019).

Jackson, T., Shenkin, A., Moore, J., Bunce, A., Van Emmerik, T., Kane, B., Burcham, D., James, K., Selker, J., Calders, K., 2019. An architectural understanding of natural sway frequencies in trees. J. R. Soc. Interface 16, 20190116.

Joffre, R., Rambal, S., Ratte, J.P., 1999. The dehesa system of southern Spain and Portugal as a natural ecosystem mimic. Agroforest. Syst. 45, 57–79.

Khosravipour, A., Skidmore, A.K., Isenburg, M., Wang, T., Hussin, Y.A., 2014. Generating pit-free canopy height models from airborne lidar. Photogramm. Eng. Remote Sens. 80, 863–872.

Lau, A., Calders, K., Bartholomeus, H., Martius, C., Raumonen, P., Herold, M., Vicari, M., Sukhdeo, H., Singh, J., Goodman, R.C., 2019. Tree biomass equations from terrestrial LiDAR: A case study in Guyana. Forests 10, 527.

Lecigne, B., Delagrange, S., Messier, C., 2017. Exploring trees in three dimensions: VoxR, a novel voxel-based R package dedicated to analysing the complex arrangement of tree crowns. Ann. Bot. 121, 589–601.

Lefsky, M.A., Cohen, W.B., Parker, G.G., Harding, D.J., 2002. Lidar remote sensing for ecosystem studies. Bioscience 52, 19–30.

Levick, S.R., Asner, G.P., 2013. The rate and spatial pattern of treefall in a savanna landscape. Biol. Conserv. 157, 121–127.

Levick, S.R., Baldeck, C.A., Asner, G.P., 2015. Demographic legacies of fire history in an African savanna. Funct. Ecol. 29, 131–139.
Levick, S.R., Richards, A.E., Cook, G.D., Schatz, J., Guderle, M., Williams, R.J., Subedi, P., Trumbore, S.E., Andersen, A.N., 2019. Rapid response of habitat structure and above-ground carbon storage to altered fire regimes in tropical savanna. Biogeosciences 16, 1493–1503.
Lin, Y., Hyyppä, J., Jaakkola, A., 2010. Mini-UAV-borne LIDAR for fine-scale mapping. IEEE Geosci. Remote Sens. Lett. 8, 426–430.
Liu, K., Shen, X., Cao, L., Wang, G., Cao, F., 2018. Estimating forest structural attributes using UAV-LiDAR data in Ginkgo plantations. ISPRS J. Photogramm. Remote Sens. 146, 465–482.
Luo, Y., El-Madany, T., Ma, X., Nair, R., Jung, M., Weber, U., Filippa, G., Bucher, S.F., Moreno, G., Cremonese, E., Carrara, A., Gonzales-Cascon, R., Cáceres Escudero, Y., Galvagno, M., Pacheco-Labrador, J., Martín, M.P., Perez-Priego, O., Reichstein, M., Richardson, A.D., Menzel, A., Römermann, C., Migliavacca, M., 2020. Nutrients and water availability constrain the seasonality of vegetation activity in a Mediterranean ecosystem. Global Change Biol. 26, 4379–4400.
Marini, R.P., 2009. Physiology of pruning fruit trees. Virginia Cooperative Extension Publication 422-025. https://vtechworks.lib.vt.edu/bitstream/handle/10919/55299/422-025.pdf?sequence=1&isAllowed=y (accessed 20.11.2019).
Martin, D., Vázquez-Piqué, J., Alejano, R., 2015. Effect of pruning and soil treatments on stem growth of holm oak in open woodland forests. Agroforest. Syst. 89, 599–609.
Mattheck, C., 1998. Design in nature: learning from trees. Springer, Berlin Heidelberg.
Mattheck, C., Tesari, I., 2004. The mechanical self-optimisation of trees. In: Collins, M. W., Brebbia, C.A. (Eds.), Design and Nature II. WIT Press, Southampton.
Mayor, X., Rodà, F., 1994. Effects of irrigation and fertilization on stem diameter growth in a Mediterranean holm oak forest. For. Ecol. Manage. 68, 119–126.
McMahon, T., 1973. Size and shape in biology: elastic criteria impose limits on biological proportions, and consequently on metabolic rates. Science 179, 1201–1204.
Moreno, G., Cubera, E., 2008. Impact of stand density on water status and leaf gas exchange in Quercus ilex. For. Ecol. Manage. 254, 74–84.
Moskal, L.M., Zheng, G., 2011. Retrieving forest inventory variables with terrestrial laser scanning (TLS) in urban heterogeneous forest. Remote Sens. 4, 1–20.
Muir, J., Phinn, S., Eyre, T., Scarth, P., 2018. Measuring plot scale woodland structure using terrestrial laser scanning. Remote Sens. Ecol. Conserv. 4, 320–338.
Naidoo, L., Cho, M.A., Mathieu, R., Asner, G., 2012. Classification of savanna tree species, in the Greater Kruger National Park region, by integrating hyperspectral and LiDAR data in a Random Forest data mining environment. ISPRS J. Photogramm. Remote Sens. 69, 167–179.
Nair, R.K.F., Morris, K.A., Hertel, M., Luo, Y., Moreno, G., Reichstein, M., Schrumpf, M., Migliavacca, M., 2019. N: P stoichiometry and habitat effects on Mediterranean savanna seasonal root dynamics. Biogeosciences 16, 1883–1901.
Olofsson, K., Holmgren, J., Olsson, H., 2014. Tree stem and height measurements using terrestrial laser scanning and the RANSAC algorithm. Remote Sens. 6, 4323–4344.
Perez-Priego, O., El-Madany, T.S., Migliavacca, M., Kowalski, A.S., Jung, M., Carrara, A., Kolle, O., Martín, M.P., Pacheco-Labrador, J., Moreno, G., 2017. Evaluation of eddy covariance latent heat fluxes with independent lysimeter and sapflow estimates in a Mediterranean savannah ecosystem. Agric. For. Meteorol. 236, 87–99.
Plieninger, T., Modolell y Mainou, J., Konold, W., 2004. Land manager attitudes toward management, regeneration, and conservation of Spanish holm oak savannas (dehesas). Landscape Urban Plann. 66, 185–198.
Pommerening, A., Grabarnik, P., 2019. Theories and concepts in individual-based forest ecology. In: Individual-based Methods in Forest Ecology and Management. Springer International Publishing, Cham, pp. 21–49.
Popescu, S.C., Wynne, R.H., Scrivani, J.A., 2004. Fusion of small-footprint lidar and multispectral data to estimate plot-level volume and biomass in deciduous and pine forests in Virginia, USA. For. Sci. 50, 551–565.
Popescu, S.C., Zhao, K., 2008. A voxel-based lidar method for estimating crown base height for deciduous and pine trees. Remote Sens. Environ. 112, 767–781.
Poulter, B., Frank, D., Ciais, P., Myneni, R.B., Andela, N., Bi, J., Broquet, G., Canadell, J. G., Chevallier, F., Liu, Y.Y., Running, S.W., Sitch, S., van der Werf, G.R., 2014. Contribution of semi-arid ecosystems to interannual variability of the global carbon cycle. Nature 509, 600.
Pulido, F., Moreno, G., García, E., Obrador, J.J., Bonal, R., Díaz, M., 2013. Resource manipulation reveals flexible allocation rules to growth and reproduction in a Mediterranean evergreen oak. J. Plant Ecol. 7, 77–85.
Pulido, F.J., Díaz, M., Hidalgo de Trucios, S.J., 2001. Size structure and regeneration of Spanish holm oak Quercus ilex forests and dehesas: effects of agroforestry use on their long-term sustainability. For. Ecol. Manage. 146, 1–13.
Pulkkinen, M., 2012. On non-circularity of tree stem cross-sections: effect of diameter selection on cross-section area estimation, Bitterlich sampling and stem volume estimation in Scots pine. Silva Fenn. 46, 747–986.
Putman, E.B., Popescu, S.C., 2018. Automated estimation of standing dead tree volume using voxelized terrestrial Lidar data. IEEE Trans. Geosci. Remote Sens. 56, 6484–6503.
QGIS Development Team, 2019. QGIS Geographic Information System. Open Source Geospatial Foundation Project.
R Development Core Team, 2017. R: A language and environment for statistical computing. https://www.R-project.org/.
rapidlasso GmbH, 2007-2019. LAStools. https://rapidlasso.com/lastools/.
Raumonen, P., Kaasalainen, M., Åkerblom, M., Kaasalainen, S., Kaartinen, H., Vastaranta, M., Holopainen, M., Disney, M., Lewis, P., 2013. Fast automatic precision tree models from terrestrial laser scanner data. Remote Sens. 5, 491–520.
Ravaglia, J., Fournier, R.A., Bac, A., Véga, C., Côté, J.-F., Piboule, A., Rémillard, U., 2019. Comparison of three algorithms to estimate tree stem diameter from terrestrial laser scanner data. Forests 10, 599.
Reineke, L.H., 1933. Perfection a stand-density index for even-aged forest. J. Agric. Res. 46, 627–638.
Riegl Laser Management Systems GmbH, 2015. Riegl VZ 2000 Data Sheet. https://www.laserscanning-europe.com/de/system/files/redakteur_images/DataSheet_VZ-2000_2015-03-24.pdf. (accessed 15.11.2019).
Rivest, D., Rolo, V., López-Díaz, M.L., Moreno, G., 2011. Belowground competition for nutrients in shrub-encroached Mediterranean dehesas. Agricultural Nutrient Cycling in Agroecosystems 90, 347.
Sheppard, J., Morhart, C., Hackenberg, J., Spiecker, H., 2016. Terrestrial laser scanning as a tool for assessing tree growth. iForest 10, 172–179.
Shiklomanov, A.N., Bradley, B.A., Dahlin, K.M., M Fox, A., Gough, C.M., Hoffman, F.M., M Middleton, E., Serbin, S.P., Smallman, L., Smith, W.K., 2019. Enhancing global change experiments through integration of remote-sensing techniques. Front. Ecol. Environ. 17, 215-224.
Singh, J., Levick, S.R., Guderle, M., Schmullius, C., Trumbore, S.E., 2018. Variability in fire-induced change to vegetation physiognomy and biomass in semi-arid savanna. Ecosphere 9, e02514.
Solla, A., García, L., Pérez, A., Cordero, A., Cubera, E., Moreno, G., 2009. Evaluating potassium phosphonate injections for the control of Quercus ilex decline in SW Spain: implications of low soil contamination by Phytophthora cinnamomi and low soil water content on the effectiveness of treatments. Phytoparasitica 37, 303–316.
Srinivasan, S., Popescu, S.C., Eriksson, M., Sheridan, R.D., Ku, N.-W., 2015. Terrestrial laser scanning as an effective tool to retrieve tree level height, crown width, and stem diameter. Remote Sens. 7, 1877–1896.
Stovall, A.E., Vorster, A.G., Anderson, R.S., Evangelista, P.H., Shugart, H.H., 2017. Non-destructive aboveground biomass estimation of coniferous trees using terrestrial LiDAR. Remote Sens. Environ. 200, 31–42.
Sun, Y., Liang, X., Liang, Z., Welham, C., Li, W., 2016. Deriving merchantable volume in poplar through a localized tapering function from non-destructive terrestrial laser scanning. Forests 7, 87.
Terradas, J., 1999. Holm oak and holm oak forests: an introduction. In: Caldwell, M.M., Heldmaier, G., Lange, O.L., Mooney, H.A., Schulze, E.-.D., Sommer, U. (Eds.), Ecology of Mediterranean evergreen oak forests. Springer, Berlin, pp. 3–14.
Thorpe, H.C., Astrup, R., Trowbridge, A., Coates, K.D., 2010. Competition and tree crowns: a neighborhood analysis of three boreal tree species. For. Ecol. Manage. 259, 1586–1596.
UMS GmbH, D1 Permanent tree girth band user manual. http://www.labcell.com/media/127951/d1%20manual.pdf (accessed 23.06.2020).
Valladares, F., Guzmán, B., 2006. Canopy structure and spatial heterogeneity of understory light in an abandoned Holm oak woodland. Ann. For. Sci. 63, 749–761.
van Leeuwen, M., Nieuwenhuis, M., 2010. Retrieval of forest structural parameters using LiDAR remote sensing. Eur. J. Forest Res. 129, 749–770.
Verbeeck, H., Bauters, M., Disney, M., Calders, K., 2019. Time for a plant structural economics spectrum. Frontiers in Forests and Global Change 2, 43.
Wade, J.E., Hewson, E.W., 1979. Trees as a local climatic wind indicator. J. Appl. Meteorol. 18, 1182–1187.
Yao, W., Krzystek, P., Heurich, M., 2012. Tree species classification and estimation of stem volume and DBH based on single tree extraction by exploiting airborne full-waveform LiDAR data. Remote Sens. Environ. 123, 368–380.
Yu, X., Hyyppä, J., Kukko, A., Maltamo, M., Kaartinen, H., 2006. Change detection techniques for canopy height growth measurements using airborne laser scanner data. Photogramm. Eng. Remote Sens. 72, 1339–1348.
Zimbres, B., Shimbo, J., Bustamante, M., Levick, S., Miranda, S., Roitman, I., Silvério, D., Gomes, L., Fagg, C., Alencar, A., 2020. Savanna vegetation structure in the Brazilian Cerrado allows for the accurate estimation of aboveground biomass using terrestrial laser scanning. For. Ecol. Manage. 458, 117798.